CHINESE OPTICS LETTERS

Vol. 20, No. 6 | June 2022

Single-wall carbon nanotube assisted all-optical wavelength conversion at 2.05 μm

Zonghui Tao (陶宗慧), Wanzhuo Ma (马万卓)*, Lei Du (杜 垒), Xin Li (李 鑫), Yan Lou (娄 岩), Tianshu Wang (王天枢), and Huilin Jiang (姜会林)**

College of Opto-Electronic Engineering, Changchun University of Science and Technology, Changchun 130022, China

*Corresponding author: mawz@cust.edu.cn

**Corresponding author: HLjiang@cust.edu.cn

Received January 26, 2022 | Accepted March 18, 2022 | Posted Online April 29, 2022

We fully demonstrate the special requirements of a mid-infrared all-optical wavelength converter. The construction mechanism of a 2.05 μm all-optical wavelength converter based on the single-wall carbon nanotube (SWCNT) is proposed. Systematic experiments are carried out, and the converter device is successfully developed. With the assistance of SWCNT-coated microfiber, the conversion efficiency up to −45.57 dB is realized, and the tuning range can reach 9.72 nm. The experimental results verify the correctness of the proposed mechanism and the feasibility of the converter device so that it can be a new technical approach for all-optical wavelength conversion beyond 2 μm. We believe the research can extend the application of this composite waveguide in the field of all-optical communication.

Keywords: all-optical wavelength conversion; single-wall carbon nanotube; 2.05 μm; microfiber; fiber laser.
DOI: 10.3788/COL202220.060602

1. Introduction

Recently, the optical communication at the 2 μm band has attracted wide attention for its eye-safe characteristic and high transmittance in the atmosphere[1,2]. According to Mie scattering, the scattering intensity of near-infrared laser transmission in the atmosphere is inversely proportional to the square of the wavelength; hence, the 2 μm laser has higher potential in free-space optical communication than the conventional 1.55 μm laser[2]. In particular, the thulium-doped fiber amplifier (TDFA) exhibits ultra-broad bandwidth around 2 μm, which can be used as a promising waveband to tackle the problem of the overloaded information transmitted in the conventional communication band. However, limited by the performance of 2 μm band lasers, it is still a challenge to achieve high-speed signal processing such as wavelength division multiplexing and all-optical switching at this band. It also increases the difficulty of high-speed information transmission in this waveband. As a significant optical communication device for wavelength division multiplexing and all-optical switching, the all-optical wavelength converters have been widely concerned. Wavelength conversion allows better utilization of the network resources under a dynamic traffic pattern[3]. Therefore, the technology of wavelength conversion can be used to effectively ease wavelength blocking. There have been many methods to achieve all-optical wavelength conversion such as four-wave-mixing (FWM), cross-gain modulation (XGM), and cross-phase modulation (XPM)[4,5]. Among these, the FWM method is an attractive way because it is transparent to modulation format, capable of transmitting high bit-rate signals, with virtually instantaneous response of the Kerr nonlinearity of fused silica, and multi-channel conversion characteristics compared with the other methods[6–9]. As a result, the all-optical wavelength converter based on the FWM effect has irreplaceable advantages.

Unfortunately, conventional all-optical wavelength conversion mechanisms such as highly nonlinear fiber, semiconductor optical amplifier, and semiconductor laser have shown insufficient nonlinearity or large loss at the 2 μm band, which are not adequate to support the high-efficiency FWM. To solve this problem, researchers have explored all-optical wavelength conversion media with a broadband response such as a waveguide of silicon and optical fiber components made of chalcogenide glass to realize all-optical wavelength conversion at 2 μm, and the tuning range can reach more than 100 nm[10–14]. However, the above methods have poor integration and a complex preparation process, which are not suitable for real high-speed communication systems. The two-dimensional (2D) materials such as graphene[15], topological insulators (TIs)[16,17], transition metal dichalcogenides (TMDs)[18–20], black phosphorus (BP)[21], and MXenes[22], have been exploited ceaselessly. The 2D materials have special electronic and optical properties and have important applications in the field of all-optical signal processing[23]. In 2012, with the help of a thin film of mechanically exfoliated

graphene, Xu *et al.* demonstrated a wavelength converter that can reach the conversion efficiency of −27 dB under the power of 34 dBm, and the tuning range is 12 nm[24]. Moreover, in 2018, Song *et al.* obtained the wavelength conversion efficiency of −63 dB and a 4.5 nm tuning range via the antimonene[25]. Right after that, in 2019, the wavelength conversion of up to −59.3 dB was achieved by their team. The wavelength tuning range can be broader than 3 nm[7]. Currently, 2D materials applied on the wavelength converters are mostly reported to be utilized at the traditional communication band of 1.55 μm. It may be limited by the higher attenuation of the optical device at 2 μm than at 1.55 μm and the insufficient nonlinearity of the wavelength conversion medium. As a result, there are few reports focusing on the 2 μm band[26].

Nevertheless, these materials that are mentioned above have some disadvantages when they are regarded as the medium of the converter. For instance, although the nonlinear refractive index of $n_2 \approx 10^{-5}\,\mathrm{cm^2\,W^{-1}}$ can be achieved, graphene and BP are easily oxidized, which may lead those performances not being stable enough[27,28]. The relatively wide band gaps of TMDs, antimonene[29], and MXenes[30,31] delimit their applications at the optical communication band[32]. Single-wall carbon nanotubes (SWCNTs) can easily be produced in the form of thin films, including three steps of nanotube growth, dispersion, and deposition processes[33]. Compared with other materials, it allows a strong electric field, long interaction length, and high optical damage threshold[34]. It exhibits a fast recovery time, chemical stability[35–37], and broad spectral range. SWCNTs also possess large modulation depth and wide operation bandwidth when samples with a large diameter distribution are used[38]. On the one hand, SWCNTs can be manufactured in relatively simple and cost-effective ways by employing spin-coating and spray-coating methods. On the other hand, SWCNTs exhibit a large third-order nonlinearity[39,40] and relatively high optics, which is an advantageous characteristic for a wavelength converter. Therefore, it is of great significance to explore all-optical wavelength conversion media with higher nonlinearity and lower loss in the 2 μm band and realize high-efficiency all-optical wavelength conversion.

In this work, an all-optical wavelength converter based on SWCNT-coated microfibers is proposed via the FWM effect. A homebuilt holmium-doped fiber laser (HDFL) is established to play a role as the pump laser. The SWCNT-coated microfiber is prepared, which can be used as a highly efficient wavelength conversion medium. The conversion efficiency can reach up to −45.57 dB, and the tuning range can reach 9.72 nm. To the best of our knowledge, it is the first time that all-optical wavelength conversion beyond 2 μm is realized with SWCNT-coated microfibers.

2. All-Optical Wavelength Conversion Mechanisms, Preparation of Pump Laser, and Conversion Medium

The working mechanism of the SWCNT-based 2.05 μm all-optical wavelength converter is as follows. A 2.05 μm band laser with a fixed wavelength is used as the signal laser (frequency f_s), and another tunable laser at this band is used as the pump laser (frequency f_p). Two lasers are simultaneously input to the all-optical wavelength conversion medium based on SWCNT-coated microfibers. When the signal and pump laser are transmitted in the all-optical wavelength conversion medium, if the phase matching condition ($\Delta k = \Delta k_W + \Delta k_M + \Delta k_{\mathrm{NL}} = 0$) is satisfied, the FWM effect will be generated, resulting in two converted lasers with frequencies of $f_x = 2f_s - f_p$ and $f_x = 2f_p - f_s$ on both sides of the signal laser and the pump laser, as shown in Fig. 1. To achieve a high-efficiency FWM effect in the 2.05 μm band, the following two technical difficulties need to be solved. One is to construct a tunable pump laser with a high side mode suppression ratio (SMSR), and the other is to prepare SWCNT-coated microfibers with low loss and high nonlinearity.

2.1. Pump laser setup

The experimental setup of the tunable HDFL as the pump laser is shown in Fig. 2. A distributed feedback (DFB) laser, which works at 1564 nm, is amplified by an erbium–ytterbium co-doped fiber amplifier (EYDFA). The amplified laser from the EYDFA is injected into a 2.5 m thulium–holmium co-doped fiber (THDF) via a 1550/2000 nm wavelength division multiplexer (WDM) 1 and operates as the source of the pump laser. The 20% port of the 20/80 optical coupler (OC) 1 is set to output the laser, and the 80% port serves as the feedback of the ring cavity. The tunable filter (TF) 1 is used to adjust the wavelength of

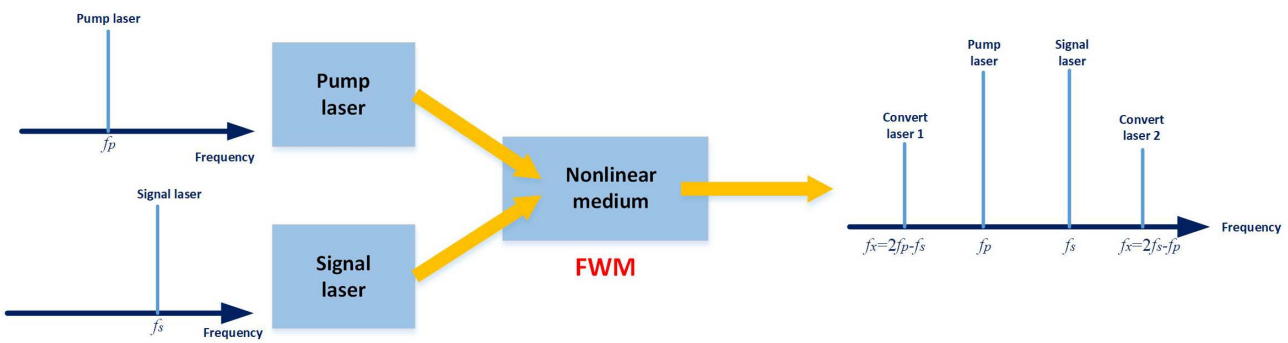

Fig. 1. Schematic diagram of all-optical wavelength conversion based on FWM.

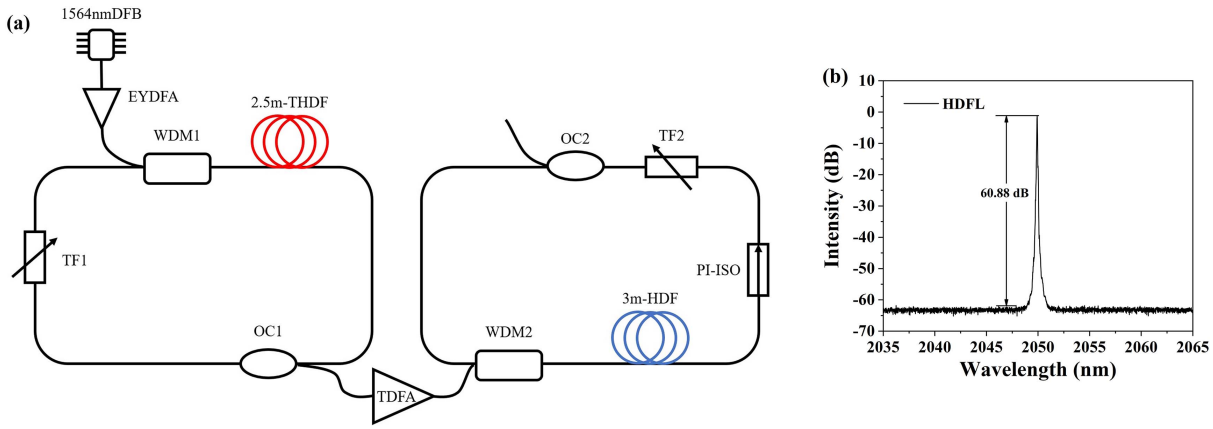

Fig. 2. (a) Schematic of Ho-doped fiber laser and (b) output spectrum.

the laser. The output laser amplified by the TDFA is considered as the pump laser and is injected into the 3 m holmium-doped fiber (HDF) through a 1950/2000 nm WDM. The polarization insensitive isolator (PI-ISO) makes sure the laser can propagate unidirectionally. TF 2 is also installed to select the wavelength of the output laser. The 90% port of a 10/90 OC is considered as the feedback of this ring cavity, and the 10% port is used for tunable laser output around 2050 nm. The experimental laser spectrum is shown in Fig. 2(b), and its SMSR can reach 60.88 dB.

2.2. Conversion medium preparation

The SWCNT-coated microfiber is prepared by the optical deposition method. The microfiber is tapered by the flame of oxyhydrogen. The length of the tapered region is about 30 mm, and the waist of the microfiber is approximately 9 μm. We install the microfiber behind the output of a fiber laser with 40 mW output power. Afterward, the SWCNT liquid, which has been pretreated by the machine ultrasonic and centrifuge, is dropped on the microfiber. When the materials of SWCNT are adhered to the microfiber, the SWCNT-coated fiber is obtained successfully, which is displayed in Fig. 3(a). One detail that affects all-optical wavelength conversion is the deposition amount of the SWCNT mass on the microfiber. Excess SWCNT will increase the attenuation and reduce the all-optical wavelength conversion efficiency. In the experiment, the deposition amount of SWCNT material can be controlled by adjusting the power of the input light source and the concentration of SWCNT dispersion. As shown in Fig. 3(b), the power via the SWCNT-coated microfiber is recorded within 100 s. One can see that the optical power instantly decreases at the beginning when the SWCNT liquid is dropped on the microfiber. Subsequently, the jitter of optical power comes soon after and later. The jitter might be caused by the change of the index of refraction instantaneously and intensely. However, the optical power will return to the level of the beginning finally, and the attenuation of 1 dB can also be measured. To test its stability, we have plotted out a figure of the relationship between the optical power and time, which is displayed in Fig. 3(c). There is no doubt that the converter has the capacity to operate steadily according to the measured results. Only ±0.08 intensity vibration occurs in 2 h.

The SWCNT has large $\chi^{(3)}$ nonlinearity and extremely short decay time so that it can be used as a highly nonlinear material for generating FWM effect[33,37]. The evanescent wave on the surface of the microfiber can interact with SWCNT to enhance the effect of the FWM effect. The characteristic of the SWCNT has been displayed in Fig. 4, which contains the figure of the Raman shift, X-ray diffraction (XRD), and absorption.

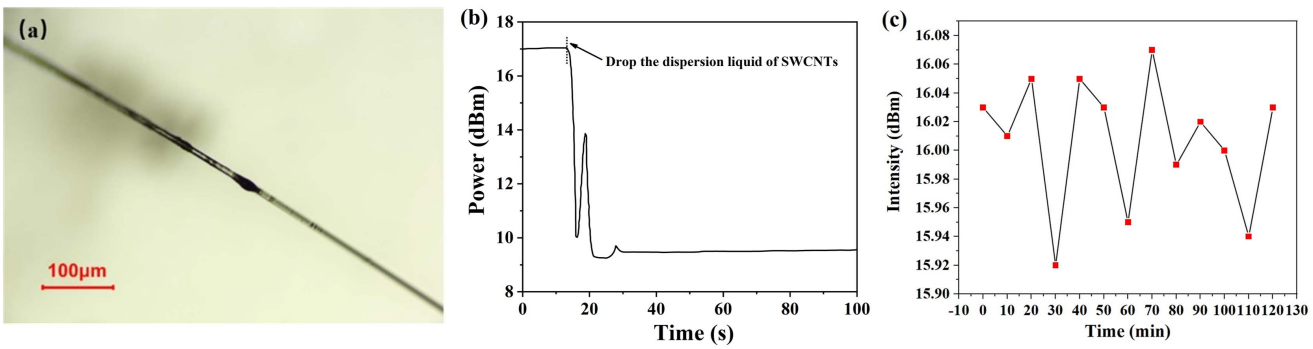

Fig. 3. (a) Microscope image of SWCNT-coated microfiber with the magnification of 100x, (b) the change of optical power through the SWCNT-coated fiber when the SWCNT liquid is dropped, and (c) the optical power jitter of the SWCNT-coated microfiber in 2 h.

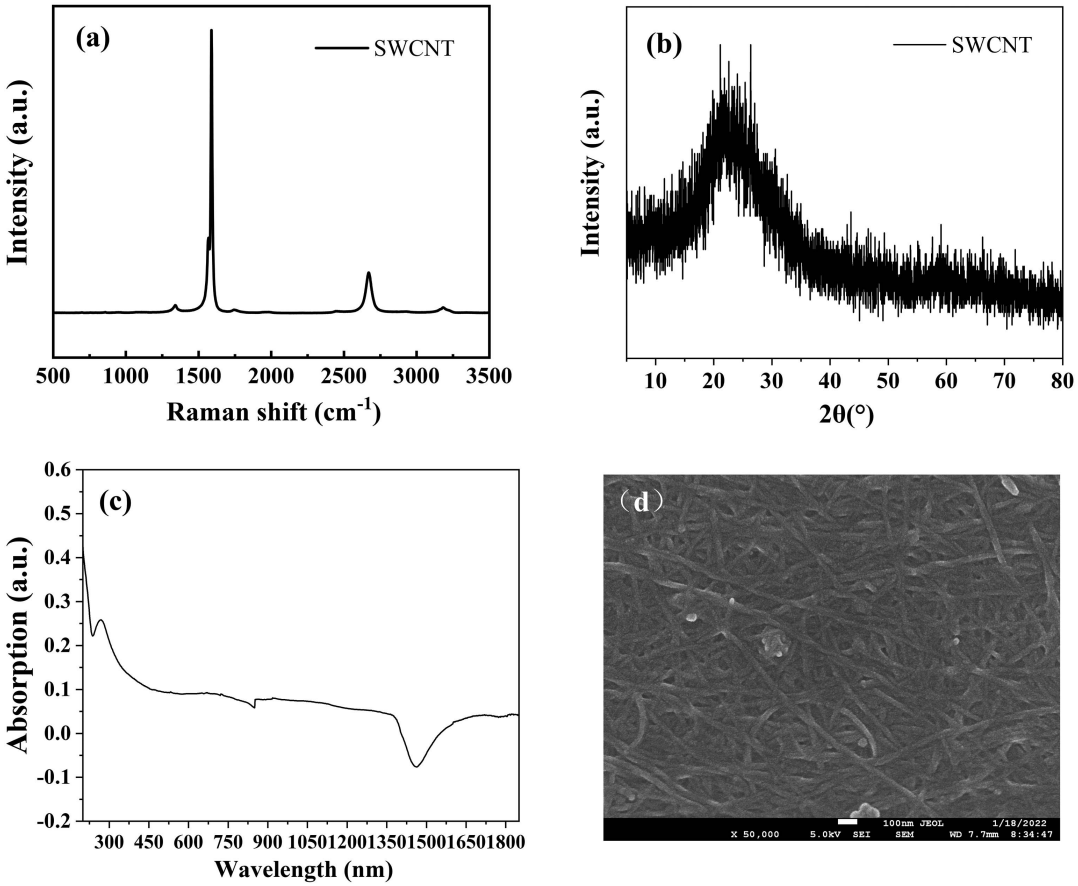

Fig. 4. Relative characteristics of SWCNT: (a) the Raman shift of the SWCNT, (b) the X-ray diffraction of the SWCNT, (c) the absorption of the SWCNT, and (d) the SEM of the SWCNT under the resolution of 100 nm.

In Fig. 4(a), the value of the primary peak is located at 1589.54 cm^{-1}, and the position of another secondary peak is at 2671.73 cm^{-1}. The results of XRD show that the angle of 2θ is 21.76° in Fig. 4(b). In Fig. 4(c), the peak value of the absorption adheres to 262.5 nm. Moreover, the diameter of this material has been displayed in Fig. 4(d), measured by the scanning electron microscope (SEM). The length of SWCNT is approximately 5–30 μm, and the outer diameter (OD) is 1–2 nm.

3. Experimental Setup

Based on the successful construction of the pump laser and the preparation of SWCNT-coated microfibers, an all-optical wavelength converter is experimentally set up, as shown in Fig. 5. The HDFL mentioned above is used for the pump laser, and the semiconductor laser operating at 2053 nm serves as the signal laser. The polarization controllers (PC1, PC2, and PC3) dominate the polarization of the pump laser and signal laser, respectively, through being adjusted with paddles. The 50/50 OC couples the pump laser and signal laser together inconveniently to input the HDF amplifier (HDFA). HDFA can be responsible for providing the gain amplification of the two bunches of the

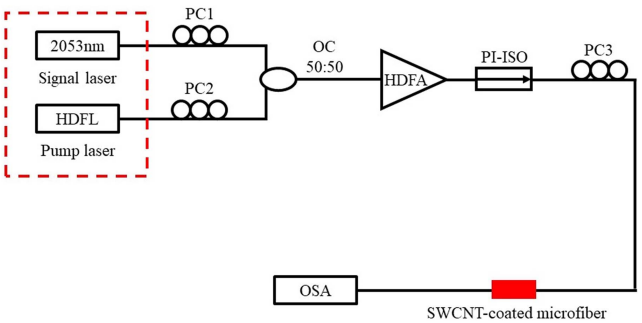

Fig. 5. Schematic of the all-optical wavelength converter.

laser. The PI-ISO in the wavelength converter can ensure that the lasers propagate unidirectionally and provide protection for the HDFA. The all-optical wavelength conversion based on the FWM effect can react at the SWCNT-coated microfiber. The results can be observed by an optical spectrum analyzer (OSA, AQ6375).

In the experiment, the TDFA is set up to 29.5 dBm to provide sufficient pump power for HDFL, and the wavelength of THDF laser is fixed at 1900 nm to match the wavelength of absorption of Ho^{3+}. The wavelength of the HDFL is firstly fixed at

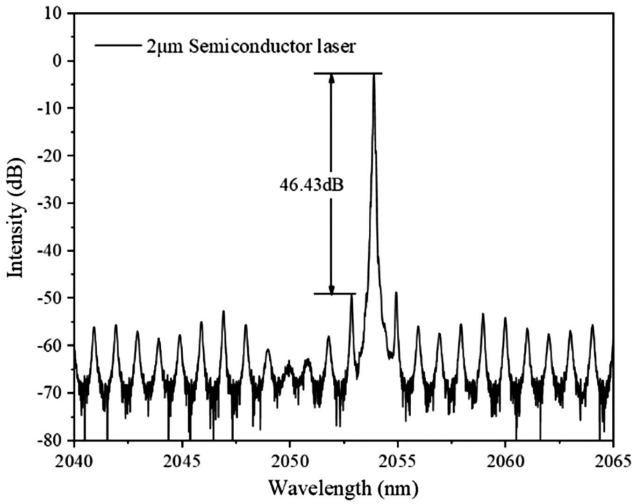

Fig. 6. Spectrum of the output laser from the 2 μm semiconductor laser.

2050.2 nm by adjusting TF 2. To obtain stable wavelength conversion states, the output power of HDFA in the wavelength converter is adjusted to 500 mW, because the phase mismatch of nonlinearity should balance the other phase mismatch of the waveguide and material to satisfy the condition of phase matching. Since the effect of FWM can be sensitive to polarization, the paddles of PCs can be regulated carefully to ensure wavelength conversion efficiency. It is worth noting that the wavelength of the semiconductor laser contains many secondary peaks, as shown in Fig. 6. This is related to the inherent properties of the semiconductor laser itself. Therefore, the SMSR of the semiconductor laser is only 46.43 dB.

4. Results and Discussion

All-optical wavelength conversion occurs at the SWCNT-coated microfiber. The FWM effect is attributed to the third-order nonlinearity of the medium, which exists in both optical fibers and nonlinear optical materials. The obtained optical spectrum is plotted in Fig. 7(a), the newly generated wavelengths are 2046 nm and 2057 nm, respectively, and the conversion efficiency up to −45.57 dB can be measured. We set a control group to prove the function of materials. If the microfiber without being decorated is added to the converter, the conversion efficiency is −50.15 dB. However, −4.58 dB improvement can be assured when the SWCNT is attached to the microfiber. We are inclined to set the different levels to show the obvious differences among the data. The reason why the pedestal of the spectrum is tilted is the non-center position of amplification via HDFA for two bunches of lasers. As a result, the SWCNT-coated microfiber can work successfully for applying to the all-optical wavelength conversion. When the wavelengths of the pump and signal lasers are fixed, the all-optical wavelength conversion efficiency shows a certain dependence on the output power of HDFA, as shown in Fig. 7(b). When the HDFA power decreases to 260 mW, the conversion efficiency decreases to −51 dB. At this time, if the power continues to decrease, the converted light will be buried in the background noise.

The wavelength conversion efficiency of FWM is related to the wavelength interval between the pump and the signal laser. Generally, the smaller the wavelength interval is, the higher the conversion efficiency is. In the wavelength domain, the relationship of the signal laser λ_s, the pump laser λ_p, and the two converted lights (λ_x and λ_c) is[7]

$$\frac{1}{\lambda_s}+\frac{1}{\lambda_p}=\frac{1}{\lambda_x}+\frac{1}{\lambda_c}. \tag{1}$$

To further investigate the performance of the wavelength converter, the relationship between the wavelength interval and the conversion efficiency is also demonstrated. Figure 8 displays the optical spectral evolution when the wavelength interval is tuned. Obviously, with the wavelength interval increasing, the conversion efficiency can decrease simultaneously. For a given signal laser with a fixed wavelength, the maximum converted

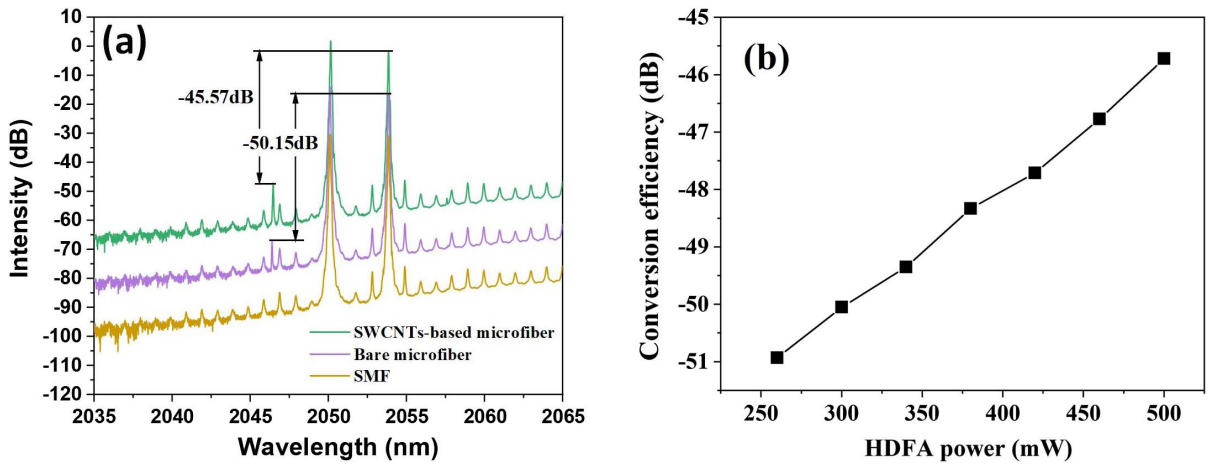

Fig. 7. (a) Experimental optical spectra of the wavelength conversion signal of the SWCNT-coated microfiber and (b) conversion efficiency as a function of HDFA power.

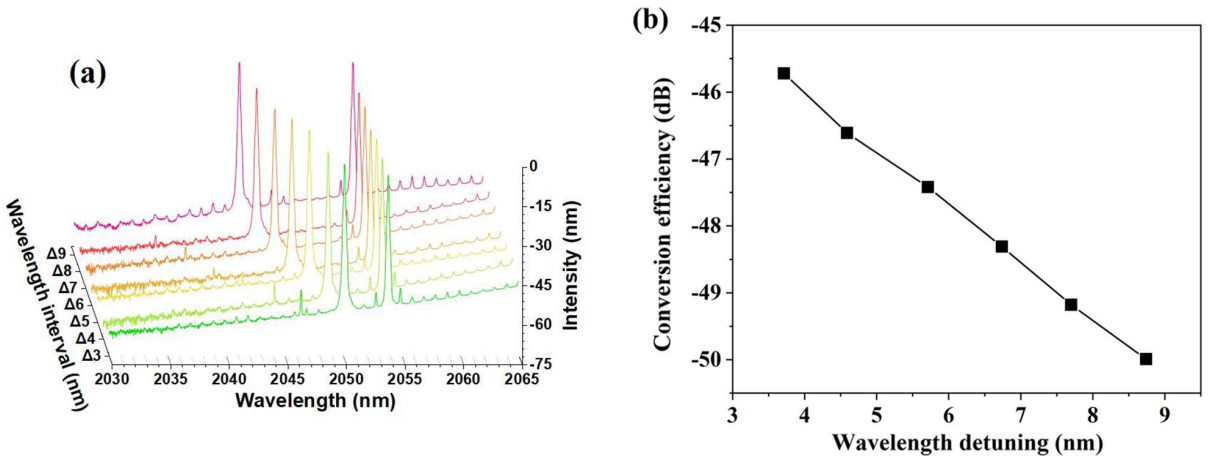

Fig. 8. (a) Wavelength conversion with different wavelength intervals and (b) wavelength conversion efficiency as a function of wavelength intervals.

wavelength interval is proved to be 9.72 nm, as shown in Fig. 8(a). When the wavelength interval decreases from 3.71 nm to 9.72 nm, the conversion efficiency decreases from −45.57 dB to −51.5 dB, as shown in Fig. 8(b). In the wavelength conversion process of loading modulation information, a narrow wavelength interval can introduce additional crosstalk. Therefore, in practical application, the conversion efficiency and intersymbol crosstalk should be combined to select the wavelength interval reasonably.

5. Conclusion

In conclusion, we have demonstrated an SWCNT-coated microfiber-based all-optical wavelength converter at 2.05 μm. To solve the problems of low efficiency and limited tuning range of the all-optical wavelength converter, a homebuilt 2050.2 nm tunable HDFL is used as the pump laser, and the SWCNT-coated microfiber is successfully obtained by an optical deposition method. The converter can realize a conversion efficiency of −45.57 dB, and the tunable wavelength interval of 9.72 nm can be achieved. To the best of our knowledge, it is the first time that the working band of an all-optical wavelength converter based on SWCNT-coated microfiber is extended beyond 2 μm. We think the research on the wavelength converter can be a reference for subsequent experiments and enrich the kinds of optical devices in the 2 μm network. However, in our opinion, the all-optical wavelength conversion efficiency needs to be further improved to provide important support for high-speed communication in the mid-infrared band.

Acknowledgement

This work was supported by the National Natural Science Foundation of China (Nos. 62005024 and 61975021), Jilin Province Young Scientific and Technological Talents Supporting Project (No. QT202104), Research Project of Jilin Provincial Education Department (No. JJKH20210816KJ), and Natural Science Foundation of Jilin Province (Nos. YDZJ202101ZYTS139 and 20190201271JC).

References

1. W. Ma, T. Wang, Y. Zhang, P. Liu, Y. Su, Q. Jia, M. Bi, P. Zhang, and H. Jiang, "Widely tunable 2 μm continuous-wave and mode-locked fiber laser," Appl. Opt. **56**, 3342 (2017).
2. P. Lin, T. Wang, W. Ma, J. Chen, Z. Jiang, and C. Yu, "2-μm free-space data transmission based on an actively mode-locked holmium-doped fiber laser," IEEE Photonics Technol. Lett. **32**, 223 (2020).
3. S. Aozasa, H. Masuda, T. Sakamoto, K. Shikano, and M. Shimizu, "Gain-shifted TDFA employing high concentration doping technique with high internal power conversion efficiency of 70%," Electron. Lett. **38**, 361 (2002).
4. Q. Xu, V. R. Almeida, and M. Lipson, "Micrometer-scale all-optical wavelength converter on silicon," Opt. Lett. **30**, 2733 (2005).
5. S. J. B. Yoo, "Wavelength conversion technologies for WDM network applications," J. Lightwave Technol. **14**, 955, (1996).
6. A. Zhang and M. S. Demokan, "Broadband wavelength converter based on four-wave mixing in a highly nonlinear photonic crystal fiber," Opt. Lett. **30**, 2375 (2005).
7. Y. Song, Y. Chen, X. Jiang, Y. Ge, Y. Wang, K. You, K. Wang, J. Zheng, J. Ji, Y. Zhang, J. Li, and H. Zhang, "Nonlinear few-layer MXene-assisted all-optical wavelength conversion at telecommunication band," Adv. Opt. Mater. **7**, 1801777 (2019).
8. R. A. Faris, S. K. Al-Hayali, and A. H. Al-Janabi, "Au coated ZnO/MWCNTs nanocomposites film-induced four-wave-mixing effect for multi-wavelength generation in erbium-doped fiber laser," Opt. Commun. **485**, 126746 (2021).
9. F. E. Durak, S. A. Sadik, K. Boumediene, M. Khelladi, and A. Altuncu, "Characterization of four wave mixing effect in dense wavelength division multiplexing systems," in *28th Signal Processing and Communications Applications Conference (SIU)*, (2020), p. 1.
10. R. K. W. Lau, M. Ménard, Y. Okawachi, M. A. Foster, A. C. Turner-Foster, R. Salem, M. Lipson, and A. L. Gaeta, "Continuous-wave mid-infrared frequency conversion in silicon nanowaveguides," Opt. Lett. **36**, 1263 (2011).
11. Q. Jin, T. Yin, Z. Tu, D. Chen, Y. Shi, D. Dai, and S. Gao, "Performance evaluation of continuous-wave mid-infrared wavelength conversion in silicon waveguides," Appl. Opt. **58**, 2584 (2019).
12. S. Zlatanovic, J. S. Park, S. Moro, J. M. C. Boggio, I. B. Divliansky, N. Alic, S. Mookherjea, and S. Radic, "Mid-infrared wavelength conversion in silicon waveguides using ultracompact telecom-band-derived pump source," Nat. Photonics **4**, 561 (2010).
13. N. A. Otman and M. Čada, "Phase-matched mid-infrared difference frequency generation using a nanostructured gallium arsenide metamaterial with nanoholes," IEEE Photonics J. **12**, 5900110 (2020).

14. Z. Tu, X. Guan, D. Chen, H. Hu, X. Wang, and S. Gao, "2 μm mid-infrared silicon-rich silicon nitride/silicon hybrid nonlinear waveguides," Opt. Commun. **481**, 126544 (2021).
15. K. S. Novoselov, A. K. Geim, S. V. Morozov, D. Jiang, Y. Zhang, S. V. Dubonos, I. V. Grigorieva, and A. A. Firsov, "Electric field effect in atomically thin carbon films," Science **306**, 666 (2004).
16. H. Zhang, C.-X. Liu, X.-L. Qi, X. Dai, Z. Fang, and S.-C. Zhang, "Topological insulators in Bi_2Se_3, Bi_2Te_3 and Sb_2Te_3 with a single Dirac cone on the surface," Nature Phys. **5**, 438 (2009).
17. Y. Xia, D. Qian, D. Hsieh, L. Wray, A. Pal, H. Lin, A. Bansil, D. Grauer, Y. S. Hor, R. J. Cava, and M. Z. Hasan, "Observation of a large-gap topological-insulator class with a single Dirac cone on the surface," Nature Phys. **5**, 398 (2009).
18. Q. H. Wang, K. Kalantar-Zadeh, A. Kis, J. N. Coleman, and M. S. Strano, "Electronics and optoelectronics of two-dimensional transition metal dichalcogenides," Nature Nanotech. **7**, 699 (2012).
19. M. Chhowalla, H. S. Shin, G. Eda, L.-J. Li, K. P. Loh, and H. Zhang, "The chemistry of two-dimensional layered transition metal dichalcogenide nanosheets," Nature Chem. **5**, 263 (2013).
20. C. Qin, Y. Gao, Z. Qiao, L. Xiao, and S. Jia, "Atomic-layered MoS_2 as a tunable optical platform," Adv. Opt. Mater. **4**, 1429 (2016).
21. X. Ling, H. Wang, S. Huang, F. Xia, and M. S. Dresselhaus, "The renaissance of black phosphorus," Proc. Natl. Acad. Sci. USA **112**, 4523 (2015).
22. A. Molle, J. Goldberger, M. Houssa, Y. Xu, S.-C. Zhang,, and D. Akinwande, "Buckled two-dimensional Xene sheets," Nature Mater. **16**, 163 (2017).
23. M. Liu, Z. W. Wei, A. P. Luo, W. C. Xu, and Z. C. Luo, "Recent progress on applications of 2D material decorated microfiber photonic devices in pulse shaping and all-optical signal processing," Nanophotonics **9**, 2641 (2020).
24. B. Xu, A. Martinez, and S. Yamashita, "Mechanically exfoliated graphene for four-wave-mixing-based wavelength conversion," IEEE Photonics Technol. Lett. **24**, 1792 (2012).
25. Y. Song, Y. Chen, X. Jiang, W. Liang, and Z. Han, "Nonlinear few-layer antimonene-based all-optical signal processing: ultrafast optical switching and high-speed wavelength conversion," Adv. Opt. Mater. **6**, 1701287 (2018).
26. L. Du, X. Ding, D. Han, L. Sui, Z. Tao, W. Ma, W. Tianshu, and Y. Wang, "1.9 μm all-optical wavelength converter based on a graphene oxide coated microfiber," Opt. Express **29**, 40286 (2021).
27. L. Wu, W. Huang, Y. Wang, J. Zhao, D. Ma, Y. Xiang, J. Li, J. S. Ponraj, S. C. Dhanabalan, and H. Zhang, "2D tellurium based high-performance all-optical nonlinear photonic devices," Adv. Funct. Mater. **29**, 1806346 (2019).
28. H. Hu, Z. Shi, K. Khan, R. Cao, W. Liang, A. K. Tareen, Y. Zhang, W. Huang, Z. Guo, X. Luo, and H. Zhang, "Recent advances in doping engineering of black phosphorus," J. Mater. Chem. **8**, 5421 (2020).
29. Y. Wang, W. Huang, C. Wang, J. Guo, F. Zhang, Y. Song, Y. Ge, L. Wu, J. Liu, J. Li, and H. Zhang, "An all-optical, actively *Q*-switched fiber laser by an antimonene-based optical modulator," Laser Photonics Rev. **13**, 1800313 (2019).
30. Q. Wu, Y. Wang, W. Huang, C. Wang, Z. Zheng, M. Zhang, and H. Zhang, "MXene-based high-performance all-optical modulators for actively *Q*-switched pulse generation," Photon. Res. **8**, 1140 (2020).
31. W. Huang, C. Ma, C. Li, Y. Zhang, L. Hu, T. Chen, Y. Tang, J. Ju, and H. Zhang, "Highly stable MXene (V_2CT_x)-based harmonic pulse generation," Nanophotonics **9**, 2577 (2020).
32. J. Zheng, Z. Yang, S. Chen, Z. Liang, X. Chen, R. Cao, Z. Guo, K. Wang, Y. Zhang, J. Ji, M. Zhang, and D. Fan, "Black phosphorus based all-optical-signal-processing: toward high performances and enhanced stability," ACS Photonics **4**, 1466 (2017).
33. S. Yamashita, "Nonlinear optics in carbon nanotube, graphene, and related 2D materials," APL Photonics **4**, 034301 (2019).
34. J. Liu, Y. Wang, Z. Qu, and X. Fan, "2 μm passive *Q*-switched mode-locked Tm^{3+}:YAP laser with single-walled carbon nanotube absorber," Opt. Laser Technol. **44**, 960 (2012).
35. W. B. Cho and F. Rotermund, "Carbon-nanotube-based bulk solid-state lasers," in *Woodhead Publishing Series in Electronic and Optical Materials* (2013), p. 144.
36. S. Hitosugi, W. Nakanishi, T. Yamasaki, and H. Isobe, "Bottom-up synthesis of finite models of helical (*n*,*m*)-single-wall carbon nanotubes," Nat. Commun. **2**, 492 (2011).
37. H. Kataura, Y. Kumazawa, Y. Maniwa, I. Umezu, S. Suzuki, Y. Ohtsuka, and Y. Achiba, "Optical properties of single-wall carbon nanotubes," Synth. Met. **103**, 2555 (1999).
38. Y. Chen, T. Lu, G. Wang, X. Zhang, N. R. Raravikar, Y. Zhao, L. S. Schadler, and P. M. Ajayan, "Ultrafast optical switch properties of single-wall carbon nanotube polymer composites at 1.55 μm," in *Conference on Lasers and Electro-Optics* (2002), paper CFH4.
39. J. Wang, X. Liang, G. Hu, Z. Zheng, S. Lin, D. Ouyang, X. Wu, P. Yan, S. Ruan, and Z. Sun, "152 fs nanotube-mode-locked thulium-doped all-fiber laser," Sci. Rep. **6**, 28885 (2016).
40. B. Xu, M. Omura, M. Takiguchi, A. Martinez, T. Ishigure, S. Yamashita, and T. Kuga, "Carbon nanotube/polymer composite coated tapered fiber for four wave mixing based wavelength conversion," Opt. Express **21**, 3651 (2013).